



Effect of Cr₂O₃ on the ¹⁸O tracer incorporation in SOFC materials

Martin Finsterbusch^{a,b,*}, Alexandre Lussier^a, Ezana Negusse^a, Zihua Zhu^c, Richard J. Smith^a, Juergen A. Schaefer^b, Yves U. Idzerda^a

^a Montana State University, Bozeman, MT 59717, USA

^b Technische Universitaet Ilmenau, 98693 Ilmenau, Germany

^c EMSL, Pacific Northwest National Laboratory, Richland, WA 99354, USA

ARTICLE INFO

Article history:

Received 17 November 2009

Received in revised form 2 February 2010

Accepted 3 March 2010

Keywords:

SOFC

Cr₂O₃

YSZ

LSCF

¹⁸O

Diffusion

ABSTRACT

Investigations of the impact of Cr₂O₃ overlayers on the oxygen self diffusion in two SOFC materials were conducted to gain insight into the Cr poisoning mechanism at the cathode side of solid oxide fuel cells (SOFCs) with stainless steel interconnects. High density Y_{0.15}Zr_{0.85}O₂ (YSZ) and La_{0.6}Sr_{0.4}Co_{0.2}Fe_{0.8}O₃ (LSCF) sintered pellets were covered with 3 to 30 nm Cr overlayers that were subsequently oxidized, forming Cr₂O₃. Standard ¹⁸O tracer diffusion experiments at 800 °C were performed and ToF-SIMS profiling revealed that the oxygen ion diffusion coefficients were unaffected by the thin Cr₂O₃ overlayers, which is predictable since they are a bulk property, but the extracted effective surface exchange coefficients varied with Cr₂O₃ overlayer thickness. Solid-state reaction measurements and electronic structure considerations concerning the surface exchange, led to the conclusion that the observed oxygen uptake hindrance for Cr₂O₃ capped LSCF and the slight increase of the surface exchange coefficient for Cr₂O₃ capped YSZ can be attributed to the electronic properties of Cr₂O₃. A critical thickness for Cr₂O₃ was determined to be 12 nm where the transition from decreasing cathode-performance to a Cr₂O₃-property-governed regime occurs.

© 2010 Elsevier B.V. All rights reserved.

1. Introduction

Over the past decade, solid oxide fuel cells (SOFCs) have been extensively studied to increase performance and durability while reducing operating temperature [1,2]. The main motivations for lowering the operating temperature are to enable the use of inexpensive metallic rather than ceramic interconnects [3], and to mitigate the various degradation effects [4]. Examples from previous works include anode poisoning from fuel contaminants [5], interface degradation between the electrolyte and cathode layers [6,7], and self-poisoning of the cathode by sealing and interconnect materials [8,9]. Although degradation mechanisms for cell performance have been proposed for the anode (e.g. sulfur [5]) and for electrolyte/cathode interfaces [6,7], a clear picture of the cathode degradation mechanisms due to poisoning from interconnect and sealing materials is still absent.

Deposition of contaminants and reactions between SOFC materials forming non ion-conductive oxides (like Sr_xZr_{1-x}O₂ or Cr₂O₃) have been thought to be responsible for cathode degradation since the first cell stack tests with stainless steel interconnects [10]. These interconnects are destined to remain ubiquitous because of the reduced material and machining costs. The presence of 18–22 wt.% of Cr is

necessary to match the coefficient of thermal expansion (CTE) with other cell components and for corrosion resistance via the formation of a protective Cr₂O₃ layer. Unfortunately, volatile Cr also poisons the cell.

A known poisoning mechanism at the cathode side involves the Cr₂O₃ protective layer [11] where, facilitated mainly by moisture contained in the air, gaseous Cr(OH)₂O₂ forms and diffuses throughout the gas at the cathode side. Extensive studies, using commercially available cells with stainless steel interconnects, found Cr₂O₃ clusters that originated from the reduction of Cr(OH)₂O₂ directly on the cathode material or at the triple phase boundaries (TPB) [8–10]. These deposits were identified to be responsible for a relatively fast degradation of 1% (voltage degradation) per 1000 h for state-of-the-art SOFC stacks using metallic interconnects [4]. The exact process of the deposition is still controversial, as pointed out by Jiang and Zhen [9]. Mitigation strategies are being explored, mainly by application of protective interconnect coatings [12]. Still, the controversy remains as to whether the Cr₂O₃ deposition is electrochemical in nature [11,13] or if it is a nucleation-governed reaction [9,14]. Recent publications showed evidence of a nucleation-dominated process facilitated by nucleation agents rather than competing electrochemical reactions of O₂ and Cr(OH)₂O₂ at the tri-phase boundaries (TPB) [9]. Nonetheless, a quantitative and qualitative picture of the effects of a Cr₂O₃ layer on oxygen diffusion in the cell is still absent.

In this work, the effect of a Cr₂O₃ layer on the oxygen incorporation into the electrolyte material Y_{0.15}Zr_{0.85}O₂ (YSZ), and on the cathode

* Corresponding author. 264 EPS Bldg. Physics Dept., Bozeman, MT 59717, USA. Tel.: +1 406 994 7830.

E-mail address: finsterbusch@physics.montana.edu (M. Finsterbusch).

material $\text{La}_{0.6}\text{Sr}_{0.4}\text{Co}_{0.2}\text{Fe}_{0.8}\text{O}_3$ (LSCF), was investigated to determine its influence on oxygen transport. Since both materials are oxides, ^{18}O tracer diffusion experiments were performed and the diffusion profiles were extracted by ToF-SIMS. In a second set of experiments, the solid-state reaction of both materials with Cr_2O_3 at operating temperature (800 °C) and at sintering temperature (1400 °C) was investigated using X-ray Diffraction (XRD). The results of these experiments helped determine whether the rate limitation of the oxygen exchange is due to the concentration of electronic species available on the surface (Lane and Kilner [15]) or caused by secondary phase formation (commonly found in YSZ/LSCF [16]).

2. Experimental

2.1. Sample preparation

All samples were prepared using commercially available powders, $\text{La}_{0.6}\text{Sr}_{0.4}\text{Co}_{0.2}\text{Fe}_{0.8}\text{O}_3$ (5.4 m²/g) from Fuel Cell Materials (FCM) and $\text{Y}_{0.15}\text{Zr}_{0.85}\text{O}_2$ (TZ-8YS) from TOSOH. The powders were uniaxially pressed into pellets and sintered at 1400 °C for 2 h. Sample densities were measured by the Archimedes method using ethanol as submerging liquid and found to be ~98% theoretical density for YSZ, and ~95.4% theoretical density for LSCF with the remaining 4.6% consisting approximately of 1.6% open pores and 3% closed pores (an additional weight measurement of the wet sample with the assumption of only a very thin film of ethanol on the surface but all open pores filled with ethanol yielded the approximate values for open and closed porosities). XRD measurements showed no secondary phases. Subsequently, the samples were polished on both sides with SiC sandpaper (up to 1200 grit). All samples were annealed for 8 h at 800 °C in air, to achieve sample and surface equilibria after polishing. This annealing step ensures that appropriate boundary conditions are achieved for fitting Crank's solution to the diffusion equation [17] and extracting reliable oxygen diffusion and surface exchange coefficients.

2.2. Cr film deposition

The chromium deposition was performed by means of thermal evaporation on only one side of a subset of samples in a high vacuum chamber using a tungsten basket as evaporation crucible filled with 99.996% pure Cr flakes (Alpha Aesar). The base pressure in the chamber was 1×10^{-6} Torr and reached $\sim 5 \times 10^{-6}$ Torr during the Cr depositions. A Cr film growth rate of approximately 1 nm/min was kept for all samples. To obtain uniform thicknesses, the Cr was grown simultaneously on LSCF and YSZ polished substrates as well as on a 0.5×0.5 mm piece of Si (100) with the native surface oxide intact. Sample sets with different Cr film thicknesses of 2.4, 5.4, 10.5, 12.6, 15.4 and 18.9 nm (as determined by Rutherford backscattering spectroscopy (RBS) on the Si specimen) were prepared.

To oxidize the Cr film prior to the ^{18}O experiment, every sample was annealed in air for 3 h at 800 °C. The RBS measurements showed that the films were completely oxidized and expanded to 3.6, 8.2, 16.3, 21.4, 29.8 and 38.1 nm which is in good agreement with the theoretically expected expansion value of 178%. The chemical state of the chromium oxide was determined using X-ray absorption spectroscopy (XAS in total electron yield mode) at beam line U4B of the National Synchrotron Light Source of Brookhaven National Laboratories. In Fig. 1, the upper spectra represent two different thicknesses of the as-deposited Cr films on Si after exposure to air. These two spectra represent the native oxide of the metallic Cr films due to exposure to air since the escape depth of the electrons is very small (~nm), nevertheless most of the film is metallic. The lower spectra are from a Cr film on Si after the oxidizing anneal and a 99% pure Cr_2O_3 reference powder (Alpha Aesar), demonstrating that the oxidized film is present as Cr_2O_3 . The completeness of the Cr_2O_3 film

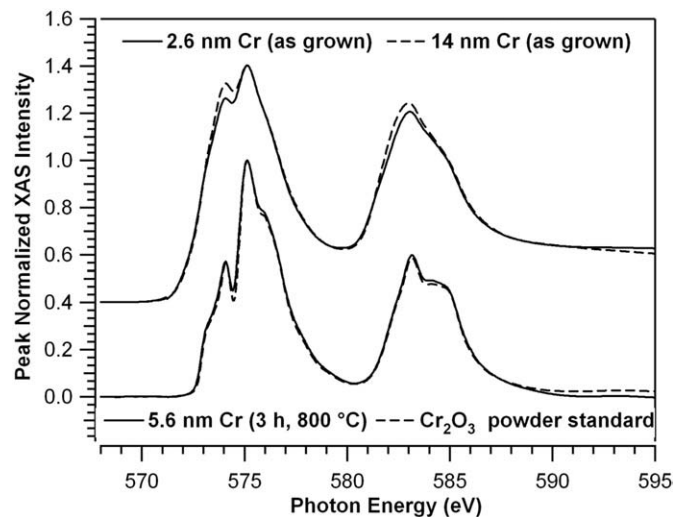


Fig. 1. XAS spectra of the chromium $L_{2,3}$ -edges of two as-deposited Cr films after exposure to air (upper spectra, offset for clarity) and a film oxidized for 3 h at 800 °C (solid line of lower spectra). Also shown is a Cr_2O_3 powder reference (dashed line of lower spectra).

on the LSCF and YSZ samples (polished) was ensured by EDX mapping of Cr and Fe in a 50×50 μm area in a field-emission scanning electron microscope image for the thinnest Cr_2O_3 film (3.6 nm) on a LSCF substrate. It showed a uniform Cr coverage demonstrating that the thin films are complete. The high resolution FE-SEM picture of an annealed sample showed a compact and crystalline film with grain sizes around and slightly larger than the film thickness (20–100 nm for the 29.8 nm Cr_2O_3 film).

2.3. ^{18}O tracer diffusion

A standard tracer diffusion setup was built, as in [18], in order to carry out the ^{18}O tracer diffusion experiments. A tube furnace with a quartz tube sealed at one end containing the samples was heated up to 800 °C in air at ambient pressure. After annealing the samples for 3 h the quartz tube was evacuated down to $\sim 5 \times 10^{-5}$ Torr and a 1:1 isotopic mixture of ^{18}O and ^{16}O (from Icon Isotopes) was backfilled into the system to reestablish the initial standard O_2 partial pressure. The atmosphere was monitored using a quadrupole mass spectrometer (QMS) to detect possible ^{18}O depletion due to the isotopic exchange with the sample. Neither ^{18}O depletion nor a change of pressure in the quartz tube was observed. The exchange gas isotopic ratio was constant at 50% ^{18}O for all samples and all three species $^{16}\text{O}_2$, $^{18}\text{O}^{16}\text{O}$ and $^{18}\text{O}_2$ were equally abundant (within the detection limit of our QMS). After 30 min the oven was retracted from the quartz tube and the samples were quenched to ~ 100 °C in approximately 2 min to minimize additional oxygen exchange.

2.4. Depth profiling by SIMS

The cross-sectional SIMS measurements were performed at Pacific Northwest National Laboratory (PNNL) using an IONTOF V ToF-SIMS spectrometer. A standard SIMS sample preparation was used [18] to measure the ^{18}O depth profile. All samples were cut in half using a diamond saw and the exposed cross-sections polished with SiC sandpaper (up to 1200 grit). To remove surface contaminations from the polishing, the cross-section was pre-sputtered with 1.0 keV Cs^+ ions until a steady state ToF-SIMS spectrum was achieved. Next, 25 keV Bi^+ ions were focused into a ~ 4 μm diameter spot and rastered over a 15×15 μm^2 area during data acquisition. Measurements were taken at 25 μm steps along the sample's cross-section. A low primary ion (Bi^+) current was used to avoid signal saturation ($^{16}\text{O}^- \leq 0.1$

counts per shot) with the noise level of the ^{18}O signal $<0.01\%$ of its peak intensity.

2.5. Solid-state reaction with Cr_2O_3

Additional experiments were conducted to ascertain that no substantial solid-state interaction between Cr_2O_3 and YSZ or LSCF occurred. One-to-one volume ratio mixtures of Cr_2O_3 powder (Alpha Aesar, 99.9% pure) and powders of both materials of interest were prepared to determine the XRD patterns of any possible secondary phase formation. Each mixture was ground until a uniform color was achieved. For each mixture, 4 different pellets were uniaxially pressed. One pellet was sintered for 7 h at 800°C , another for 14 h at 800°C , and a third for 2 h at 1400°C . Each pellet was then polished using diamond sandpaper (3 M–45 μm grains) and investigated by XRD.

3. Results

A typical ^{18}O depth profile obtained by cross-section SIMS (symbols) and the corresponding fit (solid lines) can be seen in Fig. 2. The normalized concentration $C'(x)$ after a 30 min exposure at 800°C is plotted as a function of the depth, x , with the surface at $x=0$. Both, the bare side and Cr_2O_3 film side of one sample are displayed (here the Cr_2O_3 film is too thin to be represented on this scale). Since only one side of each pellet is coated with Cr_2O_3 , the remaining bare side is used as the uncoated baseline reference. Comparing the diffusion coefficient, D_T , and the surface exchange coefficient, k , values of the bare side of each film thickness provides an easy check for repeatability and to ensure the differences in the effective surface exchange values are only due to the Cr_2O_3 layer. An important check on the appropriateness of the fitting procedure as well as the simplification for thin films (see Discussion) is that the extracted values for the diffusion coefficient, D_T , should be the same for both sides of the pellet, bare and Cr_2O_3 covered, because D_T represents a bulk property of YSZ and LSCF. In general, YSZ has a higher diffusion coefficient, D_T , but much smaller surface exchange coefficient, k , than LSCF. For both materials, constant D_T values and similar k values (of the bare sides) were extracted which are very close to those reported in the literature ($D_T=3.0\times 10^{-8}\text{ cm}^2\text{ s}^{-1}$ and $k=8.0\times 10^{-6}\text{ cm s}^{-1}$ for LSCF [19] and $D_T=6.5\times 10^{-8}\text{ cm}^2\text{ s}^{-1}$ and $k=4.0\times 10^{-8}\text{ cm s}^{-1}$ for YSZ [18]).

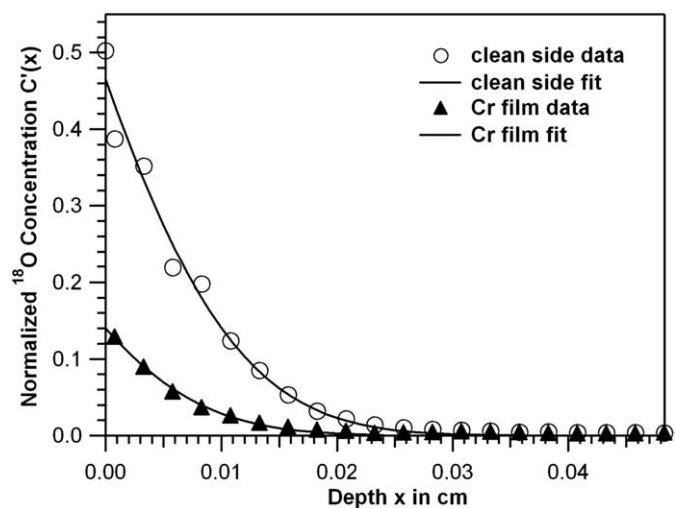


Fig. 2. ^{18}O concentration depth profile and the corresponding fit for both sides of a LSCF pellet, one side uncovered (open circles) and one side covered by a 4.4 nm thick Cr_2O_3 overlayer (filled triangles).

4. Discussion

4.1. Diffusion parameters

For isotopic exchange anneals, the diffusion of the tracer through a solid gas interface into a semi-infinite medium is described by Crank's solution of the diffusion equation [20],

$$C'(x) = \frac{C(x,t) - C_{\text{bg}}}{C_{\text{gas}} - C_{\text{bg}}} = \text{erfc}\left(\frac{x}{2\sqrt{D_T t}}\right) - \exp\left(\frac{k \cdot x}{D_T} + \frac{k^2 \cdot t}{D_T}\right) \times \text{erfc}\left(\frac{x}{2\sqrt{D_T t}} + k \cdot \sqrt{\frac{t}{D_T}}\right) \quad (1)$$

where $C'(x)$ is the normalized tracer concentration, $C(x,t)$ is the measured tracer concentration at depth x after annealing time t , C_{gas} is the tracer concentration in the gas and C_{bg} is the tracer's background concentration. This equation applies directly to the bare side of our samples since there is only the gas–LSCF or gas–YSZ interface. For the bare sides the surface exchange coefficient, k (in $\text{cm} \cdot \text{s}^{-1}$) and the diffusion coefficient, D_T (in $\text{cm}^2 \cdot \text{s}^{-1}$) represent intrinsic properties of the LSCF and YSZ which can be directly derived from Eq. (1) by fitting the measured ^{18}O tracer diffusion profile using a non-linear least square fit. The boundary conditions associated with this solution can be found elsewhere [17] and must be carefully maintained (e.g. constant ^{18}O concentration in the gas). When a Cr_2O_3 film is present on the surface of the substrate, the model is more complicated since we have two interfaces. First the gas–solid interface at the surface of the sample (gas– Cr_2O_3), second the interface between the film and the substrate (Cr_2O_3 –LSCF or Cr_2O_3 –YSZ).

For the Cr_2O_3 covered sides the oxygen molecule must first diffuse through the Cr_2O_3 before entering the substrate. If we use Eq. (1) for fitting the profile – the extracted parameter k represents an effective surface exchange coefficient which depends on the following parameters: $k_{\text{Cr}_2\text{O}_3}$, the surface exchange coefficient for Cr_2O_3 , $D_{\text{O-Cr}_2\text{O}_3}$, the diffusion coefficient of oxygen in Cr_2O_3 and $k_{\text{Cr}_2\text{O}_3/\text{substrate}}$ the transfer of oxygen through the Cr_2O_3 /substrate interface. With the additional complication of surface roughness and Cr_2O_3 thickness variations, possible diffusion of Cr into or secondary phase formation with the substrate, attempting to derive a complete equation for the surface exchange coefficient utilizing these parameters might be generally useful but not feasible for our study since some of these parameters are very sample specific and difficult to measure. Furthermore, the goal of this study is to get a first impression of the impact of Cr_2O_3 on the oxygen uptake. Instead, since the thickness of the Cr_2O_3 overlayer is very small compared to the total diffusion length (e.g. 30 nm film thickness compared to $\sim 300\ \mu\text{m}$ total diffusion length in YSZ) an effective surface exchange coefficient is used k_{eff} . Using this approach, one might consider 3 possible regimes where 3 different rate determining steps govern the behavior of k_{eff} as we increase the Cr_2O_3 overlayer thickness. First a regime where k_{eff} is mainly determined by the change in electronic structure at the surface due to the increase in Cr_2O_3 overlayer thickness, second (once a stable electronic structure of the surface is established) a regime where k_{eff} is now mainly controlled by the flux of oxygen through the Cr_2O_3 /substrate interface and for very thick films a third regime where k_{eff} is controlled by the diffusion of oxygen through the Cr_2O_3 (this regime would violate our assumption that the film thickness is small compared to the diffusion length and therefore is inaccessible with our experiment).

In Fig. 3 the extracted D_T values are plotted versus Cr_2O_3 layer thickness for each side of the samples for LSCF and YSZ. The bare sides of the Cr coated samples are represented by the multiple data points at $x=0$. The values for the Cr_2O_3 covered sides are plotted with increasing Cr_2O_3 -film thickness. As expected, the diffusion coefficient, D_T , is identical for both the clean and Cr_2O_3 covered side, as highlighted by the average D_T value (solid line for LSCF, dashed line

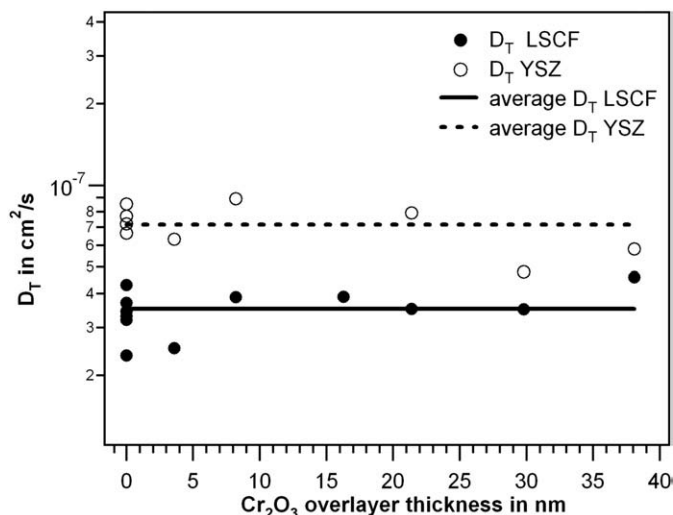


Fig. 3. D_T values for LSCF (filled circles) and YSZ (open circles) as function of Cr_2O_3 overlayer thickness.

for YSZ). This is strong evidence that our k_{eff} assumption holds. The effective surface exchange coefficients for Cr_2O_3 covered LSCF and YSZ are plotted in Fig. 4, also as a function of increasing Cr_2O_3 -film thickness. (Again the direct surface exchange coefficients for clean LSCF and YSZ are plotted as zero Cr_2O_3 coverage.) The most striking feature for Cr_2O_3 coated LSCF is the rapid decrease of the effective surface exchange coefficient, k_{eff} , by over one order of magnitude. Exponential fits with respect to thickness (since the true mechanisms are unknown, as first approximation a single process with a governing energy barrier is used) indicate that k_{eff} for Cr_2O_3 coated LSCF (solid line) approaches an asymptotic value that is lower than the asymptotic value of the YSZ fit (dashed line). This also highlights the most striking feature of the YSZ data – an increasing k_{eff} for increasing Cr_2O_3 -film thickness, which eventually exceeds the LSCF values.

4.2. Cause of inhibited oxygen uptake

To understand the cause of inhibited oxygen uptake, it is first of all necessary to distinguish between rate limitation due to the concentration of electronic species available at the surface, as suggested by Lane and Kilner [15] for the GDC system and by various other authors for the mixed conducting perovskites like doped SrTiO_3 and LSF/LSCF

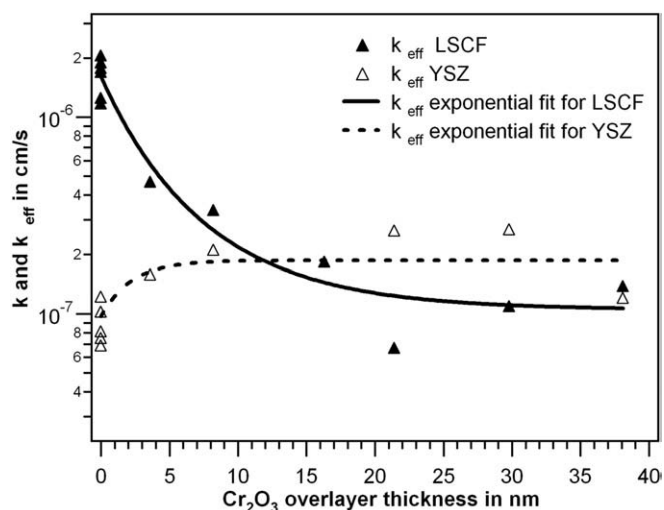


Fig. 4. k and k_{eff} values for LSCF (filled triangles) and YSZ (open triangles) as function of Cr_2O_3 overlayer thickness.

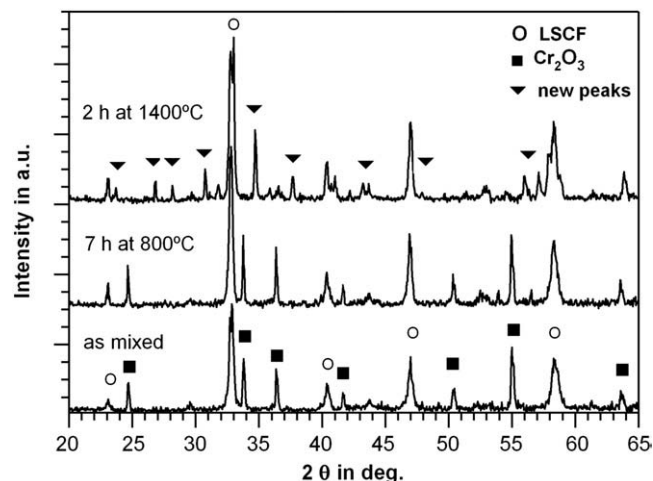


Fig. 5. XRD spectra of the LSCF- Cr_2O_3 1:1 mixture before (lower spectrum), after 7 h annealing at 800°C in air (middle spectrum), and after 2 h annealing at 1400°C in air (upper spectrum).

[21–23], and secondary phase formation at the interface of film and substrate as commonly found in the YSZ/LSCF system [16]. To check for the formation of secondary phases, a mixture of Cr_2O_3 /LSCF and Cr_2O_3 /YSZ was prepared (see Experimental) and sintered at 800°C for 7 h in air, an annealing time twice the actual annealing time of the tracer diffusion studies to account for the modest detection limit of XRD. To check for possible long-term secondary phase formation, samples were also sintered at 1400°C for 2 h. In Fig. 5 the XRD spectra are shown for the 1:1 mixture of LSCF and Cr_2O_3 as prepared (lower spectrum), the mixture after 7 h at 800°C (middle), and after 2 h at 1400°C (upper spectrum). The LSCF peaks (circles) and Cr_2O_3 peaks (squares) identified in the “as mixed” spectrum are also observed in the “7 h at 800°C ” annealed spectrum. No additional peaks were observed for annealing at 800°C , indicating that no secondary phase formed after 7 h. However, for the “2 h at 1400°C ” anneal spectrum the chromia related peaks are completely absent and new peaks can be observed (triangles), indicating that a secondary phase formation occurred. In contrast, the XRD spectrum for a mixture of YSZ and Cr_2O_3 (not shown) showed no additional peaks even after sintering for 2 h at 1400°C . Thus, secondary phase formation can be eliminated as a contributing factor to the extracted ^{18}O diffusion.

4.3. Rate limitations

Differentiating between rate limitations due to oxygen adsorption at the surface or to the electronic properties of the Cr_2O_3 overlayer is rather difficult as shown for mixed conductors by Adler et al. [23]. It is also discussed by Lane and Kilner [15] for wide band gap materials like GDC, using the same band gap arguments as Adler et al. In our case LSCF at 800°C is a mixed conductor with an electronic conductivity of about $\sigma = 100 \text{ S cm}^{-1}$ [24]. Cr_2O_3 , is considered a semiconductor at high temperatures ($E_g = 3.3 \text{ eV}$ at 1300°C [25]) with a conductivity of $\sigma = 0.002 \text{ S cm}^{-1}$ at 800°C [26]. Considering these differences in the electronic properties (almost semimetal vs. band gap) and the small crystal size (on the order of film thickness) and thus the large amount of grain boundaries which are mostly perpendicular to the surface, the decrease in the surface exchange coefficient for LSCF covered with Cr_2O_3 is most likely due to the reduction in available electronic species rather than limitations in the adsorption, which is usually related to the number of active sites on the surface [23]. This is especially interesting since Cr_2O_3 is still an electronic conductor, allowing electrons from the LSCF to aid in the reduction of oxygen at the surface even after the electronic structure of the film has completely formed. As Cr_2O_3 overlayer thickness increases further these contributions become

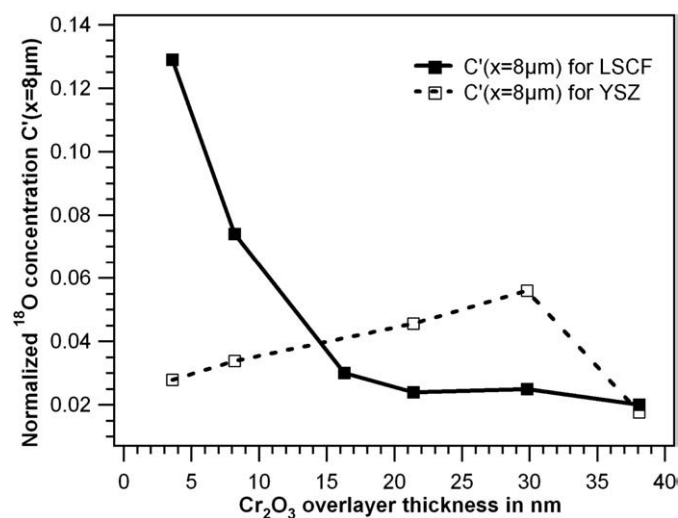


Fig. 6. Near surface concentration of ^{18}O ($x=8\ \mu\text{m}$) for LSCF (filled squares) and YSZ (open squares).

smaller and smaller leading to a slower decrease in k_{eff} for LSCF than increase for YSZ as observed in Fig. 4.

In contrast, since YSZ is a poor electronic conductor with a very high band gap ($E_{\text{g}}=4.23\ \text{eV}$ for 9.5% Y at room temperature [27] and $\sigma\approx 0.001\ \text{S cm}^{-1}$ for polycrystalline YSZ at 800 °C [28]), this assumption predicts that for our nanocrystalline Cr_2O_3 on YSZ there would be an increase in the surface exchange coefficient with increasing Cr_2O_3 overlayer thickness. This increase would continue until the electronic structure of the Cr_2O_3 is established completely. In Fig. 4, the k_{eff} value increases with increasing Cr_2O_3 thickness and reaches a constant value of approximately 2 times its clean surface value for thicknesses above 12 nm.

Interestingly, the asymptotic value for k_{eff} for Cr_2O_3 on YSZ is even higher than that for Cr_2O_3 on LSCF. This is confirmed in the measured ^{18}O concentration near the surface for the two. Fig. 6 plotted the normalized concentration of ^{18}O vs. Cr_2O_3 -film thickness for the cross-section measurement nearest to the surface (at $x=8\ \mu\text{m}$). It clearly shows that the concentration of ^{18}O in YSZ with Cr_2O_3 overlayer thicknesses above 12 nm is larger than for LSCF with the same Cr_2O_3 -film thickness. This is strong evidence that at these thicknesses the diffusion through the Cr_2O_3 /substrate interface ($k_{\text{Cr}_2\text{O}_3/\text{substrate}}$) is the governing mechanism. A possible explanation for the lower k_{eff} values for LSCF might be the existence of a very thin layer of a secondary phase right at the interface of the Cr_2O_3 grains and the LSCF substrate. This very thin layer is not detectable with the experimental methods employed in our study and thus cannot be excluded. Furthermore no secondary phases are likely to form at an YSZ/ Cr_2O_3 interface leaving the k_{eff} values for YSZ unaffected. Other possible explanations could include the difference in activation energy for vacancy hopping, since LSCF has a much higher activation energy compared to YSZ (resulting in the difference in their D values in Fig. 3). However, since the surface electronic structure of the Cr_2O_3 film is well established at these overlayer thicknesses, the total oxygen uptake by, and subsequent diffusion into, the substrate would be controlled by the Cr_2O_3 /substrate interface in any case.

These results provide a possible explanation of the different degradation behaviors of LSCF vs. LSM cathodes observed by others [29–31]. Jiang and Zhen [9] concluded that for LSCF/GDC cells, Cr_2O_3 preferentially deposits on the cathode. Based on this work, this preferential deposition would rapidly decrease the cathode's electrocatalytic activity. However, in LSM/YSZ cells, Jiang found that Cr_2O_3 preferentially deposits on the electrolyte, which based on our results leads to a slight increase of the oxygen uptake directly into the YSZ and only a gradual degradation is observed for low current densities [29]. For further understanding of the degradation processes taking

place in an operating fuel cell the conditions at the air side would have to be mimicked better as gaseous chromium is deposited and, as pointed out earlier, might have additional effects on the oxygen uptake related to the deposition mechanism (e.g. electrochemical reaction competing with the oxygen reduction vs. nucleation [9]).

5. Conclusions

The model systems Cr_2O_3 /LSCF and Cr_2O_3 /YSZ which are, according to Jiang and Zhen [9], the most reasonable choices regarding the causes for degradation in SOFCs with metallic interconnects were investigated. The Cr_2O_3 layer thickness dependence of the effective surface exchange coefficient k_{eff} was measured and a critical thickness of $\sim 12\ \text{nm}$ was established, above which the oxygen incorporation is governed by the electronic properties of Cr_2O_3 and the diffusion through the Cr_2O_3 /substrate interface. The formation of secondary phases was found to occur at temperatures and annealing times far higher than those used in our diffusion studies but cannot be completely ruled out as a contributing factor when comparing different substrates. We conclude that the changes in the effective surface exchange coefficient k_{eff} for Cr_2O_3 films thinner than 12 nm are due to changes in the surface electronic structure, similar to those introduced by Lane and Kilner [15] for materials with relatively high band gap. These changes improve the oxygen uptake for Cr_2O_3 covered YSZ but decrease it for LSCF (in accordance with literature [21]), especially when the Cr_2O_3 film is nanocrystalline and thus has many active sites on the surface. We also conclude from our study that for films thicker than 12 nm the interface between Cr_2O_3 and the substrate plays an important role in the oxygen uptake; but the rate determining mechanism at the interface remains unknown.

Acknowledgement

This work is supported by the Department of Energy under grant DE-08NT0004115 and by the National Science Foundation under grant CBET-0709358. Parts of this work were performed using the Environmental Molecular Sciences Laboratory (EMSL), a national scientific user facility sponsored by the Department of Energy's Office of Biological and Environmental Research and located at Pacific Northwest National Laboratory. The National Synchrotron Light Source is supported by the Department of Energy.

References

- [1] S.P. Jiang, Materials Science and Engineering A-Structural Materials Properties Microstructure and Processing 418 (1–2) (2006) 199.
- [2] L.C. De Jonghe, C.P. Jacobson, S.J. Visco, Annual Review of Materials Research 33 (2003) 169.
- [3] J.W. Fergus, Materials Science and Engineering A-Structural Materials Properties Microstructure and Processing 397 (1–2) (2005) 271.
- [4] N.H. Menzler, F. Tietz, M. Bram, I.C. Vinke, L.G.J. de Haart, Advances in solid oxide fuel cells IV, Ceramic Engineering and Science Proceedings 29 (5) (2008).
- [5] A. Lussier, S. Sofie, J. Dvorak, Y.U. Idzerda, International Journal of Hydrogen Energy 33 (14) (2008) 3945.
- [6] A. Chen, G. Bourne, K. Siebein, R. DeHoff, E.D. Wachsman, K. Jones, Journal of the American Ceramic Society 91 (8) (2008) 5.
- [7] A. Lussier, J. Dvorak, S. Stadler, J. Holroyd, M. Liberati, E. Arenholz, S.B. Ogale, T. Wu, T. Venkatesan, Y.U. Idzerda, Thin Solid Films 516 (2008) 4.
- [8] S.P. Jiang, S. Zhang, Y.D. Zhen, Journal of The Electrochemical Society 153 (1) (2006) 7.
- [9] S.P. Jiang, Y. Zhen, Solid State Ionics 179 (2008) 5.
- [10] K. Hilpert, D. Das, M. Miller, D.H. Peck, R. Weiß, Journal of The Electrochemical Society 143 (11) (1996).
- [11] S. Taniguchi, M. Kadowaki, H. Kawamura, T. Yasuo, Y. Akiyama, Y. Miyake, T. Saitoh, Journal of Power Sources 55 (1) (1995) 73.
- [12] H. Chen, J.A. Lucas, W. Priyantha, M. Koczyk, R.J. Smith, K. Lund, C. Key, M. Finsterbusch, P.E. Gannon, M. Deibert, V.I. Gorokhovskiy, V. Shutthanandan, R. Nachimuthu, Surface & Coatings Technology 202 (19) (2008) 4820.
- [13] S.P.S. Badwal, R. Deller, K. Foger, Y. Ramprakash, J.P. Zhang, Solid State Ionics 99 (3–4) (1997) 297.
- [14] E. Konyshova, H. Penkalla, E. Wessel, J. Mertens, U. Seeling, L. Singheiser, K. Hilpert, Journal of The Electrochemical Society 153 (4) (2006) A765.
- [15] J.A. Lane, J.A. Kilner, Solid State Ionics 136 (2000) 927.

- [16] J.M. Ralph, C. Rossignol, R. Kumar, *Journal of the Electrochemical Society* 150 (11) (2003) A1518.
- [17] R.A. De Souza, R.J. Chater, *Solid State Ionics* 176 (23–24) (2005) 1915.
- [18] P.S. Manning, J.D. Sirman, J.A. Kilner, *Solid State Ionics* 93 (1–2) (1996) 125.
- [19] A. Esquirol, N.P. Brandon, J.A. Kilner, M. Mogensen, *Journal of the Electrochemical Society* 151 (11) (2004) A1847.
- [20] J. Crank, *The Mathematics of Diffusion*, Oxford University Press, 1975.
- [21] M. Leonhardt, R.A. De Souza, J. Claus, J. Maier, *Journal of the Electrochemical Society* 149 (2) (2002) J19.
- [22] R.A. De Souza, *Physical Chemistry Chemical Physics* 8 (7) (2006) 890.
- [23] S.B. Adler, X.Y. Chen, J.R. Wilson, *Journal of Catalysis* 245 (1) (2007) 91.
- [24] K. Swierczek, M. Gozu, *Journal of Power Sources* 173 (2) (2007) 695.
- [25] A. Atkinson, M.R. Levy, S. Roche, R.A. Rudkin, *Solid State Ionics* 177 (19–25) (2006) 1767.
- [26] J.A. Crawford, R.W. Vest, *Journal of Applied Physics* 35 (8) (1964) 5.
- [27] V.R. Paiverneker, A.N. Petelin, F.J. Crowne, D.C. Nagle, *Physical Review B* 40 (12) (1989) 8555.
- [28] I. Kosacki, T. Suzuki, V. Petrovsky, H.U. Anderson, *Solid State Ionics* 136 (2000) 1225.
- [29] T. Komatsu, R. Chiba, H. Arai, K. Sato, *Journal of Power Sources* 176 (1) (2008) 132.
- [30] F. Tietz, V.A.C. Haanappel, A. Mai, J. Mertens, D. Stover, *Journal of Power Sources* 156 (1) (2006) 20.
- [31] Y. Matsuzaki, I. Yasuda, *Journal of the Electrochemical Society* 148 (2) (2001) A126.